THE ASTROPHYSICAL JOURNAL, 469:L21–L24, 1996 September 20

X-RAY TIMING AND SPECTRAL EVOLUTION OF CIRCINUS X-1 VERSUS ORBITAL PHASE WITH THE *ROSSI X-RAY TIMING EXPLORER*

ROBERT E. SHIREY, HALE V. BRADT, ALAN M. LEVINE, AND EDWARD H. MORGAN
Department of Physics and Center for Space Research, Massachusetts Institute of Technology, Cambridge, MA 02139; shirey@space.mit.edu
Received 1996 June 14; accepted 1996 July 9

ABSTRACT

We have carried out a study of Cir X-1 through (1) detailed sampling over a single 16.5 day intensity cycle with the *Rossi X-Ray Timing Explorer* (*RXTE*) proportional counter array and (2) complementary monitoring over six such cycles with the *RXTE* all-sky monitor (ASM). We report here the temporal and spectral evolution at nonflaring phases, during which Cir X-1 remained unusually bright (∼1.0 crab) and relatively steady. The Fourier power density spectrum of the source was observed to vary with strong correlations among low-frequency flat-topped power (≲1–10 Hz), a quasi-periodic oscillation (QPO) peak centered at 1.3–12 Hz, and a broad QPO peak centered at ∼20 Hz up to ∼100 Hz. As orbital phase increased within the cycle, the rms amplitude of the flat-topped power generally (but not monotonically) decreased while the QPO features generally evolved toward higher frequency. The 1.5–12 keV spectrum was observed to generally harden during the nonflaring phases of each of the six 16.5 day periods monitored by the ASM.

Subject headings: stars: individual (Circinus X-1) — stars: neutron — X-rays: stars

1. INTRODUCTION

Circinus X-1 exhibits complex behavior on a wide range of timescales. Most prominent is its 16.5 day intensity cycle, observed in X-rays (Kaluzienski et al. 1976), IR (Glass 1978), and radio (Whelan et al. 1977). Typically, the source is relatively steady and faint for most of the cycle. When active, once each cycle it enters a period of complex X-ray flares and dips, which on occasion can be very dramatic (see, e.g., Dower, Bradt, & Morgan 1982; Oosterbroek et al. 1995). The 16.5 day periodic behavior is believed to be the result of a highly elliptical binary orbit, in which mass transfer occurs only near periastron, leading to intermittent obscuration, partial covering, and brightening near phase zero (Murdin et al. 1980; Brandt et al. 1996). The absolute intensity and nature of the cycles vary with a timescale of several years, possibly as a result of apsidal motion or disk precession (Murdin et al. 1980; Oosterbroek et al. 1995).

A number of observations over the past decade have contributed to our understanding of the nature of this source. An optical counterpart has been securely identified as a highly reddened star that exhibits variability at the 16.5 day period (Moneti 1992). Type I X-ray bursts have been observed with *EXOSAT* (Tennant, Fabian, & Shafer 1986), thus indicating that Cir X-1 contains a low magnetic field neutron star, most likely in a low-mass X-ray binary system at a distance of 6–10 kpc (see discussion in Glass 1994). The system may be a runaway from the nearby (∼27′) supernova remnant G321.9−0.3, of age 30–100 kyr (Stewart et al. 1993).

In addition to the long-term variability related to the binary orbit, Cir X-1 exhibits variability on much shorter timescales, which are likely related to the accretion disk or neutron star itself. In particular, quasi-periodic oscillations (QPOs) have been reported at 1.4, 5–17, and 100–200 Hz (Tennant 1987, 1988). See Oosterbroek et al. (1995) for a comprehensive discussion of temporal variability from *EXOSAT* observations of Cir X-1, including a discussion of its possible relation to (and uniqueness among) other low magnetic field compact objects (see also van der Klis 1994). See Brandt et al. (1996) for a report on analyses of *ASCA* observations of the energy spectrum.

Repeated observations of Cir X-1 with the proportional counter array (PCA; 2–60 keV) of the *Rossi X-Ray Timing Explorer* (*RXTE*; see Bradt, Rothschild, & Swank 1993) have been carried out over a single 16.5 day period. Three months of *RXTE* all-sky monitor (ASM; 1.5–12 keV) data are also available. We report here the current state of the source and focus primarily upon the evolution of the emission characteristics away from the flaring activity, i.e., at phases $0.2 \lesssim \phi \lesssim 0.9$ (based on the 1991 radio ephemeris of Stewart et al. 1991). Heretofore these phases have not been systematically sampled with an instrument of large aperture. In the eccentric-binary scenario, the source would be relatively remote from the secondary during these phases. The behavior of the source during the active phases will be reported at a later time.

2. OBSERVATIONS AND RESULTS

The *RXTE* ASM consists of three coded-aperture cameras that provide intensity measurements in three energy bands (roughly 1.5–3, 3–5, and 5–12 keV) of most bright X-ray sources ∼15 times per day (Levine et al. 1996). The ASM light curves of Cir X-1 (Fig. 1*a*) show that, from 1996 February 20 to May 30, Cir X-1 remained brighter than ∼1.0 crab (74 counts s^{-1}; 1060 μJy at 5.2 keV) at all phases, except for brief intensity dips (lasting 3–20 minutes in PCA data) that were occasionally detected near phase zero. The flaring state generally begins immediately after phase zero (within the limits of ASM sampling), reaching as high as 3.3 crab and lasting 2–5 days.

The ASM data show significant spectral evolution during the nonflare phases. Hardness ratios of counts in adjacent energy channels (Figs. 1*b*, 1*c*) were found to generally increase (harden) from about phase 0.2 until phase 0.6–0.85. Beyond this point, the hardness ratios usually flatten, decrease, or dip and rise again before phase zero. Near phase zero, the ratios

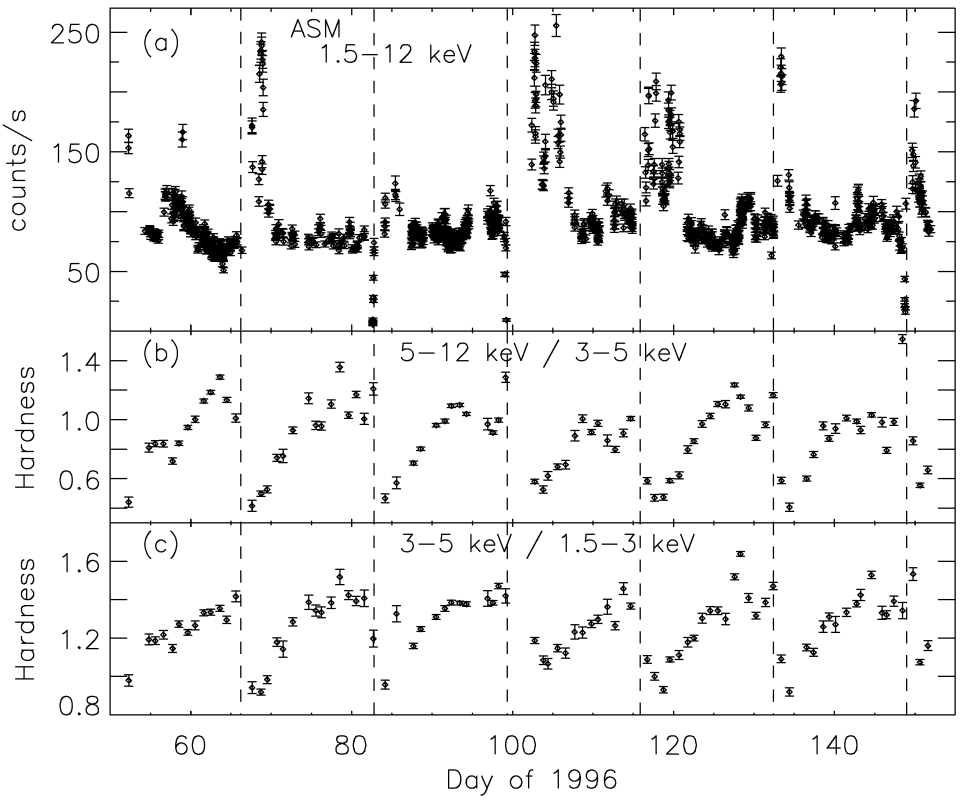

FIG. 1.—(*a*) ASM 1.5–12 keV light curve and (*b*, *c*) two hardness ratios from the three ASM energy bands. The dashed lines indicate phase zero. Each light-curve point is the average count rate from a single 90 s ASM pointing. The data points are obtained from fits to the ASM mask patterns arising from all sources in the field of view and from the background; thus the background has, in effect, been subtracted. Cir X-1 was as bright or brighter than the Crab Nebula (74 counts s^{-1}) for all six cycles shown. Each hardness point was obtained from 1 day weighted averages of the 90 s intensities. The PCA observations occurred throughout the second of these 16.5 day periods (beginning on day 66).

vary dramatically (not apparent in the 1 day averages shown) but generally become quite low during the flaring phases ($0 \lesssim \phi \lesssim 0.2$). The 1.5–12 keV count rate usually remains relatively constant during the nonflaring periods (although a decrease was observed over the first 16.5 day cycle). The hardening in the two colors ($0.2 \lesssim \phi \lesssim 0.7$) is usually due to both an increase in the 5–12 keV count rate and a decrease in the 1.5–3 keV count rate. This suggests that the energy flux from Cir X-1 increases during this period. A similar hardening pattern was observed in *Ginga* ASM data folded over the 16.5 day period (Tsunemi et al. 1989).

In 1996 March, Cir X-1 was sampled with the PCA (effective area ~7000 cm^2) 12 times during one 16.5 day orbital period. The observation times and orbital phases are summarized in Table 1, and three sample light-curve segments are shown in Figure 2. In the full PCA energy band (2–60 keV), Cir X-1 was found to be extremely active, remaining bright ($\gtrsim$1.0 crab) throughout the 16.5 day cycle (1 crab $\approx$ 13,000 counts s^{-1}). In the vicinity of phase zero (observations 1, 2, and 12), dramatic flares and dips occurred (Figs. 2*a*, 2*b*). In observation 2 (phase 0.15), the count rate climbed to more than 2.5 crab (Fig. 2*b*). Away from phase zero ($0.2 \lesssim \phi \lesssim 0.8$; observations 3–11), the count rate remained fairly steady (within 15%) at ~1.0 crab. Figure 2*c* shows a sample light curve for phase 0.5, which is typical of these observations. The source is relatively steady but exhibits flickering greatly in excess of Poisson statistics.

Two hardness ratios (5.7–22 keV/4.3–5.7 keV and 3.3–4.3 keV/2.0–3.3 keV) from the PCA count rates generally increase during the nonflaring phases as phase increases to ~0.7, beyond which the ratios are more steady. This confirms the evolution observed in the ASM data.

TABLE 1

PROPORTIONAL COUNTER ARRAY OBSERVATIONS OF CIRCINUS X-1

Observation	Day of 1996	Orbital Phase[a]
1	65.9	0.98
2	68.7	0.15
3	70.8	0.28
4	72.6	0.39
5	73.8	0.46
6	74.6	0.50
7	76.3	0.61
8	76.7	0.63
9	77.7	0.69
10	78.7	0.75
11	79.1	0.78
12	81.8	0.94

NOTES.—Each observation lasted 1–5 hr and produced 1.4–10 ks of data. Dates and phases listed are the centroids of the observations. Day 65.0 corresponds to JD 2,450,147.5.

[a] Based on the radio ephemeris of Stewart et al. 1991. Because of faint radio flares in recent years, this ephemeris is still currently in use as the best available (G. Nicolson 1996, private communication).

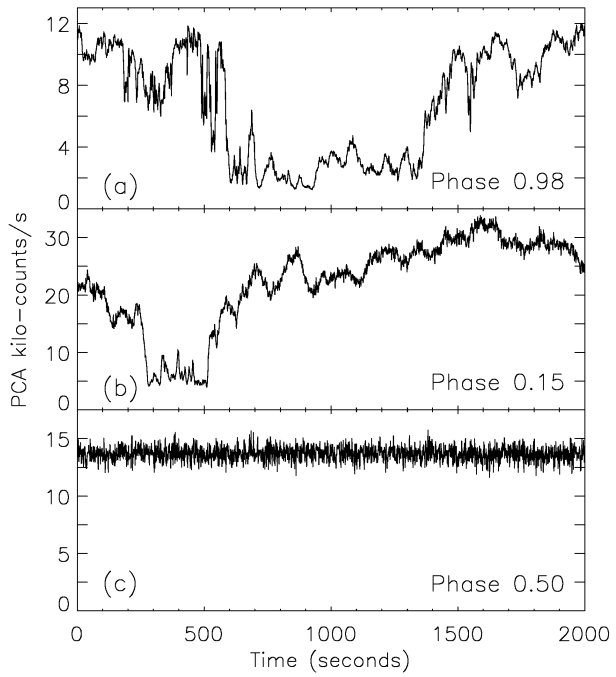

FIG. 2.—Sample PCA light curves (2–60 keV) comparing 2000 s segments, showing (*a*) strong variability and dips near phase zero (phase 0.98; observation 1), (*b*) a brighter portion of the bright flaring state 3 days later (phase 0.15; observation 2), and (*c*) a typical observation away from phase zero (phase 0.50; observation 6). Background (~100 counts s^{-1}) has not been subtracted, nor have dead-time corrections been made.

Power density spectra (PDSs) were produced from PCA data covering 2–8.6 keV in 61 μs time bins. For each 96 minute *RXTE* orbit, a continuous observation of 1–4 ks was divided into 64 s segments, and the PDS was calculated for each segment. All PDSs from the segments of a single continuous observation were averaged together, weighted by the total counts. The resulting average power spectrum from each *RXTE* orbit was then logarithmically rebinned, with dead-time–corrected Poisson noise subtracted (Zhang et al. 1995), and normalized to yield the fractional rms amplitude squared per hertz (after Belloni & Hasinger 1990b).

The PDSs from seven orbits are shown in Figure 3, offset downward by 1 decade intervals. These samples show significant low-frequency flat-topped power that cuts off above 1–10 Hz and also a QPO peak that sits on the high-frequency edge of the flat-topped power at 1.3–12 Hz (as compared to 1.4 and 5–17 Hz QPOs reported near phase zero by Tennant 1987, 1988). All the PDSs during the nonflaring phases exhibit these features. The flat-top power level systematically decreases as the cutoff and QPO frequencies increase (note that each flat-top level is more than 1 decade below the previous level in Fig. 3). Above the cutoff frequencies, the curves all track together with roughly the same power. A few PDSs not illustrated here have a steep low-frequency component below 0.1–0.4 Hz.

A broad, high-frequency QPO is also apparent in Figure 3 centered at ~20 to ~100 Hz or more. For observations in which the 1.3–12 Hz QPO frequency is below ~8 Hz, the high-frequency broad peak is always clearly present; otherwise, it is sometimes marginally detectable above 100 Hz. Note that this high-frequency QPO peak moves to higher frequencies along with the low-frequency QPO peak.

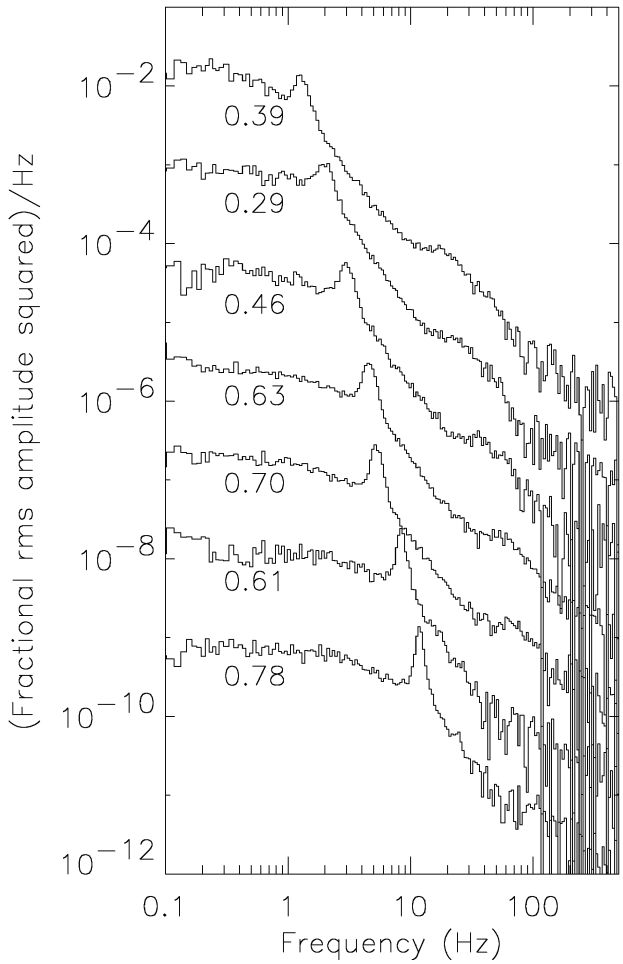

FIG. 3.—Power density spectra from seven *RXTE* orbits away from phase zero, offset downward at decade intervals. (The ordinate scale applies to the uppermost spectrum.) The curves are ordered by the frequency of the 1.3–12 Hz QPO peak and are labeled with orbital phase.

All the PDSs in the nonflaring phases were analyzed to study these trends further. The flat-topped component was fitted with a zero-centered Lorentzian profile, the two peaked features were also each fitted with a Lorentzian, and the high-frequency tail was fitted with a power law. Although the results of the fits indicate that this model is crude (via large values of the associated χ^2 statistic), the fits were adequate to determine approximate centroid frequencies and power levels. Errors (rms) for QPO centroid frequencies were estimated from 90% confidence intervals of the fits or 20% of the FWHM of the peak, whichever was greater. Errors for the flat-top power level were estimated to be ~5%. As the orbital phase increased, the power level of the flat-topped noise generally decreased (Fig. 4*a*) while the narrow QPO's frequency increased (Fig. 4*b*), in accord with the trends noted above. These trends are not monotonic, though; a large excursion occurs at $\phi = 0.4$ in both curves. Remarkably, the correlation between these two quantities (flat-top level and narrow QPO frequency) in Figure 4*c* is very strong (and negative). Moreover, the frequency of the 20–100 Hz peak scales as ~13 times the frequency of the 1.3–12 Hz peak (Fig. 4*c*), with a weak tendency for the frequency ratio to decrease (from ~16 to ~11) with increasing frequency. The frequency

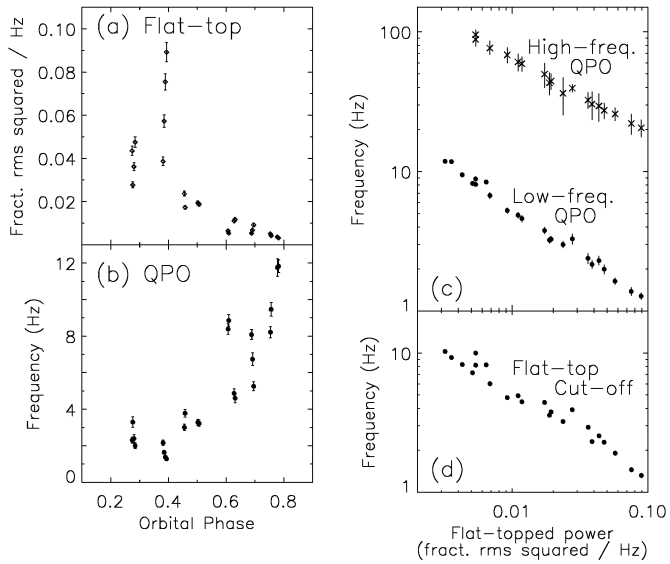

FIG. 4.—(*a*, *b*) Flat-top power level and QPO frequency, respectively, as a function of orbital phase over a single orbital cycle. (*c*) Frequency of the narrow, low-frequency QPO and the broad, high-frequency QPO vs. the flat-top power level. (*d*) Cutoff frequency of the flat-topped power vs. flat-top power level.

difference between the two peaks changes by more than a factor of 4 over this range, from less than 20 Hz to more than 80 Hz. The cutoff frequency of the flat-topped component (as measured by the width of the best-fitting zero-centered Lorentzian) also moved to higher frequency with the narrow QPO peak (Fig. 4*d*). These two frequencies agree within 20% for all observations.

3. DISCUSSION

The 1.4 and 5–17 Hz QPOs reported by Tennant et al. (1987, 1988) were found during observations near phase zero. It was suggested that the QPOs were bimodal, with the 1.4 Hz QPO independent of luminosity and the 5–17 Hz component correlated with the estimated 2–10 keV unabsorbed energy flux (Tennant 1987, 1988). Our observations show a gradual evolution of the QPO from 1.3 to 12 Hz over the *non*flaring phases. Some of the phase-zero *EXOSAT* observations that exhibited 5–17 Hz QPOs also had a QPO peak at 100–200 Hz (Tennant 1987). This low/high-frequency QPO pair is likely to be the evolving QPO pair we have observed, but extended to higher frequencies.

The correlation between the flat-top power level and the cutoff frequency (Fig. 4*d*) is similar to the effect observed by Belloni & Hasinger (1990a) in the black hole candidate Cyg X-1 and also observed in the neutron star 4U 1608−522 (Yoshida et al. 1993). In fact, several properties of 4U 1608−522 show correlations similar to those we have observed in Cir X-1. In two of the three observations of 4U 1608−522 by Yoshida et al. (1993), QPOs were seen (at 0.4 and 2.0 Hz) just above the knee in the power spectrum, and a broader peaked noise feature was observed at the higher frequencies of 1.0 and 5.1 Hz, respectively (Yoshida et al. 1993). We note that the ratio of the two peaks is the same in both observations, just as the two peaks in our Cir X-1 observations move to higher frequency with a nearly constant frequency ratio (although the ratio is different for the two sources). In both sources, the spectrum generally (but not always) hardens as these features move to higher frequencies and the flat-top power level decreases.

The *RXTE* observations of Cir X-1 have (1) confirmed a general hardening of the spectrum during the nonflaring phases 0.2–0.7, (2) demonstrated a clear trend (with moderate scatter) for the power density features to shift to higher frequency and the amplitude of the low-frequency power to decrease with increasing orbital phase during the nonflaring phases, and (3) demonstrated extremely tight correlations among the QPO features and the flat-topped power. In the eccentric-orbit model, these characteristics may reflect the evolving state of the accretion disk while it is being depleted with little or no replenishment. For example, the leveling of the hardness ratios after phase 0.6–0.8 may reflect a time constant (of order 10 days) of the disk structure. The spectral hardening and increasing QPO frequencies suggest that as the depletion occurs, the inner portion of the accretion disk, with its higher temperatures and greater Keplerian frequencies, becomes relatively more important in the emission process.

We are grateful to the entire ASM and *RXTE* engineering and science teams for their support. We thank particularly W. N. Brandt, D. Chakrabarty, J. G. Jernigan, R. Remillard, D. A. Smith, A. Tennant, and M. van der Klis for helpful discussions. Support for this work was provided by NASA contract NAS 5-30612.

REFERENCES

Belloni, T., & Hasinger, G. 1990a, A&A, 227, L33
———. 1990b, A&A, 230, 103
Bradt, H. V., Rothschild, R. E., & Swank, J. H. 1993, A&AS, 97, 355
Brandt, W. N., Fabian, A., Dotani, T., Nagase, F., Inoue, H., Kotani, T., & Segawa, Y. 1996, MNRAS, in press
Dower, R., Bradt, H., & Morgan, E. 1982, ApJ, 261, 228
Glass, I. 1978, MNRAS, 183, 335
———. 1994, MNRAS, 268, 742
Kaluzienski, L., Holt, S., Boldt, E., & Serlemitsos, P. 1976, ApJ, 208, L71
Levine, A. M., Bradt, H., Cui, W., Jernigan, J. G., Morgan, E. H., Remillard, R., Shirey, R. E., & Smith, D. A. 1996, ApJ, 469, L33
Moneti, A. 1992, A&A, 260, L7
Murdin, P., Jauncy, D. L., Haynes, R. F., Nicolson, G. D., Holt, S. S., & Kaluzienski, L. J. 1980, A&A, 87, 292
Oosterbroek, T., van der Klis, M., Kuulkers, E., van Paradijs, J., & Lewin, W. H. G. 1995, A&A, 297, 141
Stewart, R. T., Caswell, J. L., Haynes, R. F., & Nelson, G. J. 1993, MNRAS, 261, 593
Stewart, R. T., Nelson, G. J., Penninx, W., Kitamoto, S., Miyamoto, S., & Nicolson, G. D. 1991, MNRAS, 253, 212
Tennant, A. 1987, MNRAS, 226, 971
———. 1988, MNRAS, 230, 403
Tennant, A., Fabian, A. C., & Shafer, R. A. 1986, MNRAS, 221, 27P
Tsunemi, H., Kitamoto, S., Manabe, M., Miyamoto, S., & Yamashita, K. 1989, PASJ, 41, 391
van der Klis, M. 1994, ApJS, 92, 511
Whelan, J. A. J., et al. 1977, MNRAS, 181, 259
Yoshida, K., Mitsuda, K., Ebisawa, K., Ueda, Y., Fujimoto, R., & Yaqoob, T. 1993, PASJ, 45, 605
Zhang, W., Jahoda, K., Swank, J. H., Morgan, E. H., & Giles, A. B. 1995, ApJ, 449, 930